Javed, F., Hainzl, S., Aoudia, A., Qaisar, M. (2016): Modeling of Kashmir Aftershock Decay Based on Static Coulomb Stress Changes and Laboratory-Derived Rate-and-State Dependent Friction Law. - *Pure and Applied Geophysics*, *173*, 5, pp. 1559—1574.

DOI: http://doi.org/10.1007/s00024-015-1192-9

Modeling of Kashmir Aftershock Decay Based on Static Coulomb Stress Changes and Laboratory Derived Rate and State Dependent Friction Law.

F.Javed[1, 3], S. Hainzl[2], A.Aoudia[1] and M.Qaisar[4]

[1] Abdus Salam International Center for Theoretical Physics (ICTP), Trieste, Italy

[2]GFZ German Research Centre for Geosciences, Potsdam, Germany.

[3]University of Trieste, Trieste, Italy

[4]Center for Earthquake Studies (CES), National Center for Physics (NCP), Islamabad, Pakistan.

Abstract: We model the spatial and temporal evolution of October 8, 2005 Kashmir earthquake's aftershock activity using the rate and state dependent friction model incorporating uncertainties in computed coseismic stress perturbations. We estimated the best possible value for frictional resistance "$A\sigma_n$", background seismicity rate "r" and coefficient of stress variation "CV" using maximum log-likelihood method. For the whole Kashmir earthquake sequence, we measure a frictional resistance $A\sigma_n \sim 0.0185$ MPa, r ~ 20 M3.7+ events/year and CV= 0.94±0.01. The spatial and temporal forecasted seismicity rate of modeled aftershocks fits well with the spatial and temporal distribution of observed aftershocks that occurred in the regions with positive static stress changes as well as in the apparent stress shadow region. To quantify the effect of secondary aftershock triggering, we have re-run the estimations for 100 stochastically declustered catalogs showing that the effect of aftershock-induced secondary stress changes are obviously minor compared to the overall uncertainties, and that the stress variability related to uncertain slip model inversions and receiver mechanisms remains the major factor to provide a reasonable data fit.

1. INTRODUCTION

It is well known that major shallow earthquakes are followed by increased seismic activity, known as ‘aftershocks’, which last for several days to several years. The temporal decay of this aftershock activity usually follows the Omori-Utsu law and the spatial distribution can be roughly modeled by static Coulomb failure stress changes (ΔCFS). As pointed out in previous studies of mainshock-aftershock sequences in different tectonic environments, seismicity models only based on ΔCFS fail to explain the observed activation in regions where stress was apparently decreased by the mainshock (Hainzl et al., 2009; Parsons et al., 2012). However, several possible mechanisms might explain the occurrence of aftershocks in those stress shadows, e.g. dynamic stresses, secondary triggering and stress uncertainties. In particular, intrinsic variability and uncertainty of calculated stress values are shown to explain aftershock activation in regions with a negative average stress change, if laboratory-derived rate- and state-dependent friction laws are considered (Helmstetter and Shaw, 2006; Marsan 2006; Hainzl et al., 2009). We further explore this possibility by the analysis of the Mw7.6 Kashmir mainshock which occurred on 8th October, 2005 in northern Pakistan and was followed by an intense aftershock activity. In the case of Kashmir’s earthquake sequence, 30% aftershocks with magnitude ranging from 3.5 to 5.5 were occurring in the stress shadow region (see figure 1). In the paper of Parsons et al. (2012), the authors included the uncertainties related to small scale slip variability, which is also a part of the overall uncertainties, defined by Coefficient of stress variation (CV) in our study. They analyzed the spatial aftershock locations in relation to the static CFS changes, and concluded that this will explain the occurrence of aftershocks and spatial variability near the mainshock. However, they also demonstrated that it does not affect the overall regional stress change pattern, even using different values of coefficient of friction and

orientation of regional stress field. They found that half of the events that occurred in the stress shadow southwest of the mainshock can be explained by aftershock triggering, while the rest of them are ascribed to the mainshock and remained therefore unexplained. However, other factors such as the uncertainty of the mainshock source model and the receiver fault orientations are likely to dominate the overall uncertainty and variability (Cattania et al. 2014). Therefore, we compare the observed aftershock pattern with the spatiotemporal seismicity patterns predicted by the Coulomb rate- and state-dependent friction (CRS) model under consideration of involved dominant uncertainties (CV). As shown by Parsons et al. (2012), secondary triggering seems to play a role in generating the aftershocks particularly southwest of the mainshock. In this current paper, we will thus address in particular the two questions:

1) Whether the occurrence of aftershocks in stress decreased region can be explained by uncertainties of the calculated static stress changes (CV-value)?

2) How much of the stress variability can be attributed to secondary triggering?

To discuss the second point, we remove secondary aftershocks, which are obviously triggered by other aftershocks, by applying the epidemic type aftershock sequence (ETAS) model. We analyse the model forecasts for the original catalog as well as stochastically declustered catalogs in order to evaluate the model fits and the role of secondary triggering.

2. SEISMICITY MODEL

The underlying physical model that has been utilized in this study to determine the aftershock decay rate is based on laboratory-derived rate-and-state dependent friction laws (Dieterich, 1994; Dieterich et al., 2000). This model incorporates the stress

perturbations induced by earthquakes and the physical constitutive properties of the faults (Dieterich, 1994). The model parameters are, besides the background seismicity rate r, the frictional resistance $A\sigma_n$, and the relaxation time for the aftershocks t_a (or alternatively, the tectonic stressing rate $\dot{S}$)

Based on laboratory-derived rate-and state-dependent friction laws, the earthquake rate R for a population of faults is given by (Dieterich, 1994)

$$R=\frac{r}{\gamma\dot{S}}\ , \qquad (1)$$

where γ is a state variable governed by the equation

$$d\gamma=\frac{1}{A\sigma_n}\left(dt-\gamma ds\right) \qquad (2)$$

Here σ_n is the effective normal stress and A is a dimensionless fault constitutive friction parameter (Dieterich, 1994; Dieterich et al., 2000). Based on this evolution equation, the time-dependence can be explicitly calculated for stress histories consisting of coseismic stress steps and constant tectonic loading. In particular, the seismicity rate after a stress step ΔS at time t = 0 is given by (Dieterich, 1994)

$$R(t)=\frac{1}{[1+(exp(-\Delta S/A\sigma_n)-1)exp(-t/t_a)]} \qquad (3)$$

assuming the same constant tectonic stressing rate $\dot{S}$ before and after the mainshock. This takes the form of Omori-Utsu's law, $R(t) \sim (c+t)^{-p}$, with p=1 for $t << t_a$, where the aftershock relaxation time t_a is related to the stressing rate by $t_a = A\sigma_n/\dot{S}$.

2.1 Static Coulomb Stress Changes

The locally predicted seismicity rate depends on the calculated stress change ΔS in the seismogenic volume under consideration. The approach which is here adopted has been previously proposed by various scientists (King et al., 1992; Reasenberg and Simpson,

1992; Harris and Simpson, 1992; Stein and Lisowski, 1983 and Stein et al., 1981). It is based on the Coulomb failure stress that involves both normal and shear stresses on the specified target faults or optimally oriented fault planes. The decisive parameter is the Coulomb Failure Stress (CFS), which is defined as

$$\Delta CFS = \Delta\tau + \mu (\Delta\sigma_n + \Delta p) , \qquad (4)$$

where $\Delta\tau$ and $\Delta\sigma_n$ are shear and normal stress changes, Δp is the pore pressure change and μ is the coefficient of friction which ranges from 0.6 to 0.8 for most rocks (Harris, 1998). Pore pressure modifies the co-seismic stress redistribution and for that reason they are included in the basic definition of Coulomb failure function. According to Rice and Cleary (1976), the pore pressure is related to the mean stress by Skempton coefficient B under undrained condition, $\Delta p = -B\Delta\sigma_{kk}/3$, where the Skempton coefficient can vary between 0 to 1. Alternatively, it is often assumed that for plausible fault zone rheologies, the change in pore pressure becomes proportional to normal stress on faults, $\Delta p = -B\Delta\sigma_n$ (King et al., 1992; Stein and Lisowski, 1983 and Stein et al., 1981). Substituting this relation in Eq. (4) leads to

$$\Delta CFS = \Delta\tau + \mu'\Delta\sigma_n , \qquad (5)$$

with $\mu' = \mu(1-B)$ being an effective friction coefficient. Stein & Lisowski (1983) and Stein et al. (1981) have used the value $\mu' = 0.4$ in many calculations, which we also adopt in our study.

To calculate ΔCFS, also the receiver mechanisms have to be defined. Two assumptions are commonly used in this context: a) fixed fault geometry and b) optimally oriented fault plane geometry. While in the former case, focal mechanisms (i.e. strike, dip and rake) of the aftershocks are assumed to be known by e.g. well documented faults, a theoretical focal mechanism is calculated in the latter case, which is assumed to be

optimal oriented to the total stress field consisting of the regional background stress and mainshock induced ΔCFS change. We follow here the latter approach, where the magnitude and orientation of the regional stress field are taken from Parsons et al. (2006).

2.2 Approximation of Uncertainties

Stress calculations are known to be subject to large uncertainties, which have to be considered in order to get reliable model fits (Hainzl et al., 2009, 2010b; Woessner et al., 2012). If the involved uncertainties and variabilities related to earthquake slip, receiver fault orientations, and crustal properties are ignored, the estimation of the model parameters is biased, and apparent stress shadow regions are expected which do not occur if intrinsic variability is considered (Hainzl et al., 2009; Helmstetter and Shaw, 2006; Marsan, 2006).

Three slip models were published in the literature so far, for October 8, 2005 earthquake. These slip models were determined by Parsons et al. (2006), Avouac et al. (2006) and Pathier et al. (2006). The first slip models were estimated from seismological data, while the last two were inverted from geodetic measurements. We use the analytic solutions of Okada (1992) for the elastic half space to calculate ΔCFS at grid points for all three slip models assuming a shear modulus of 30 GPa.

The results are shown in figure 2. All three slip model depict the stable stress decreased region as expected (Hainzl et al., 2009; Helmstetter and Shaw, 2006; Marsan, 2006) and also mentioned by Parsons et al. (2012). We use the average ΔCFS value as best estimate of the central stress value in each location, while the variability of the three estimated ΔCFS values represents roughly the epistemic uncertainty, is included as a part of the considered uncertainties in our analysis.

Different Types of uncertainties are associated with the stress change:

i) Local stress field variations due to heterogeneities of the crustal material and pre-stress, which might influence the seismicity rate which itself influence the forecasts, but pre-stress with its orientation will also influence the receiver mechanisms/geometry and thus effect the stress perturbations , ii) Lack of knowledge of the geometry of receiver faults at depth (Hainzl et al., 2010b), iii) The direction and amplitude of regional stress field (Hardebeck and Hauksson, 2001), iv) Incalculable small scale slip variability close to the fault which cannot be directly resolved by inversion of surface data (Helmstetter et al., 2006; Marsan 2006), and v) No uniqueness of the slip model inversions.

Most of above mentioned uncertainties cannot be simply quantified in models, while other uncertainties e.g. in the slip model can be taken directly into account, if related information are available (Woessner et al., 2012). Hainzl et al., (2009) demonstrated that the variability of the stress estimation is, in a first approximation, linearly correlated to the value of the absolute mean stress change indicating that the coefficient of variation is approximately constant in space. The authors also showed that variability of the stress field (i.e. if we account both epistemic and intrinsic uncertainties) can be taken into account in the model using simplified Gaussian distributed probability density function. Please see the Table 1 and Figure 2 of Hainzl et al. (2009) for more explanations. Thus the CV-value is an effective parameter accounting not only for the slip model variation, but also the variability of receiver mechanisms, material parameters, stress heterogeneities, etc.

Figure 3a shows the stress variation is of the order of mean Coulomb stress change, which is the result of uncertainties related to different slip models and receiver fault mechanism(strike=330, dip=30, and rake=90) variations with standard deviation(20 degrees, 10 degrees and 10 degrees respectively) in the model. We also plot the stress variation corresponding to each mean stress change at the hypocenters of the aftershocks

as shown in figure 3b. These results indicate that our assumption of a linear relation between the standard deviation and the absolute value of stress is a reasonable first order approximation in our case. To account for these uncertainties in the rate-and-state dependent friction model, a Gaussian distribution is assumed with the mean value being the average stress value of the different slip models and the standard deviation is CV*mean. The observations are compared to a number N of Monte-Carlo simulations, where the stress in each sub volume is taken randomly (in our case, we consider M7.6 Kashmir earthquake, with N=250 realizations of the stress jump) from the Gaussian distribution.

2.3 Model Parameter

The rate-and-state dependent frictional nucleation model depends on the three parameters r, $A\sigma_n$ and t_a. It is very sensitive to background seismicity rate r, which is the rate of earthquakes in the absence of any stress perturbation. In general, the background activity is expected to be non-uniform due to rheological inhomogeneities of the crust. The model assumes that the state variable is at a steady state before the application of a stress perturbation, which means that it does not change with time (Dieterich 1994; Dieterich et al., 2000; Cocco et al., 2010; Hainzl et al., 2009; Hainzl et al., 2010). Indeed, it is assumed that this initial γ-value is equal to the inverse of the tectonic stressing rate. According to Eq. (1), the seismicity rate before the application of the stress perturbation is thus equal to the background rate r, associated with a temporally stationary process, which can be in principle estimated from declustered catalogs (Stiphout et al., 2010). Jouanne et al. (2011) estimated the background seismicity rate in the Kashmir region as 0.08 M3.5+ events/day. In many studies and applications of rate and state dependent model (Cocco et al., 2010; Hainzl et al., 2009; Toda and Stein, 2003), the background seismicity rate is assumed to be spatially uniform, because of the

lack of sufficient data to estimate spatial variations. Although the background activity is likely inhomogeneous in reality, the estimation of its spatial variation from few historic events is difficult and would potentially introduce additional problems. Thus we follow the previous approach and assume a spatially uniform background rate. In our case, the value of r is not fixed but results from the maximum likelihood fit (see section 2.5). However, we will see that our result is in good agreement with the previous estimation of Jouanne et al. (2011). Furthermore, it should be noted that the value of r estimated from the non-declustered catalog contains not only the background events (i.e. definition of background rate in the strict ETAS sense) but also their triggered aftershocks, so the background rate in this case refer to the time independent smoothed seismicity rate computed from the non-declustered catalog (Catalli et al., 2008; Cocco et al., 2010).

The second important parameter in the rate-and-state dependent friction model is the frictional resistance $A\sigma_n$. While the dimensionless fault constitutive friction parameter A is approximately known from laboratory experiments; ~0.01 (Dieterich 1994; Dieterich et al., 2000), the absolute value of the effective normal stress σn is mostly unknown. It is likely to depend on depth, regional tectonic stress, fault orientation, and pore pressure (Cocco et al., 2010; Hainzl et al., 2010). For simplicity, we assumed that $A\sigma_n$ is uniform over large volumes and estimated the value of $A\sigma_n$ by data fitting. Previous applications of this model indicated values of $A\sigma_n$ in a range between 0.01 and 0.2 MPa (Cocco et al., 2010; Hainzl et al., 2010).

The third parameter in the rate-and-state dependent constitutive frictional law is the tectonic loading rate $\dot{S}$. Alternatively, one can use the relaxation time t_a which determines the duration of the aftershock activity (Hainzl et al., 2010). This parameter is not well constrained from earthquake data as long as the aftershock decay is ongoing. Therefore, t_a is also determined by the maximization of the likelihood value for the

observed Kashmir aftershock sequence.

2.4 Aftershock Data

We analyzed the aftershock events, provided by the International Seismological Centre (ISC), that occurred between 330N and 360N latitude and 720E and 750E longitude (see Fig. 1a). We first selected aftershocks of magnitude ≥ 3 that occurred between the period 2005-10-08 and 2013-10-15 in the study area. According to Parsons et al. (2012), the minimum magnitude of completeness varies from 3.7 to 4.0 for the Kashmir aftershocks in the NEIC earthquake catalog as well as in the ISC catalog for the above defined study area (see Fig. 1b). We thus selected aftershocks of magnitude ≥ 3.7 for our analysis. However, we neglected aftershocks that occurred within the first 12 hours after the Kashmir earthquake to account for likely incomplete catalog recordings in the first time interval (Kagan, 2004). A total number of 693 events were recorded in the analyzed time and space interval. Other information related to semi major, semi minor axes and orientation of the error ellipsoid are given in the catalogs. In our analysis, we used this information to account for the location uncertainties.

2.5 Stochastic Declustering

It has been recognized that sub-clustering observed in aftershock sequences might be the result of aftershock-aftershock triggering (e.g. Ogata 1988 and Ogata 1992). We want to address the question of whether the corresponding aftershock-induced stress variations significantly contribute to the overall stress uncertainties. For that, we analyze the declustered aftershock sequence to focus only on aftershocks directly related to the mainshock. Several methods have been proposed for declustering a catalog (e.g. Gardner and Knopoff 1974; Zhuang et al., 2002; Zhuang et al., 2004) We apply the stochastic

declustering methodology introduced by Zhuang et al. (2002) to obtain the aftershocks directly linked to the mainshock. The method is based on the empirical ETAS model described by

$$\text{Rate}(t) = \mu + \sum_{t_i}^{t} K10^{\alpha(M-M_c)}(c + t - t_i)^{-p} f(r),$$

where parameters c and p are related to the Omori-Utsu law and K and α to the empirical productivity law (Utsu 1961), while μ is the background rate and f(r) is the normalized isotropic kernel

$$f(r) = \left({}^{q}/_{\pi}\right) d^{2q}/(d^2 + r^2)^{(1+q)}.$$

In the case of the mainshock, the spatial kernel is calculated by the normalized sum of f(r) for a large number of point-sources with a spacing of 1 km at the rupture plane (to account for the extension of the rupture). The parameters of f(r) have been set to the reasonable value q=0.5 (which corresponds to a r^{-3} decay in agreement with the static stress decay in the far field) and d=10 km as an approximation of the location error. To obtain stochastically declustered catalogs, we firstly estimated the ETAS parameters by a maximum likelihood fit of the M≥3.7 aftershocks within [0.5 1000] days (where preceding events are used to calculate the rate within this time interval) which yields: μ=0.013 [events/day], K=0.014, c=0.048 [day], α=1.07 and p=1.19. Then single declustered catalogs were constructed by selecting randomly events according to their probability to be not triggered by another aftershock. In this way, we have created 100 stochastically declustered catalogs based on the parameters estimated by the ETAS model fit.

2.6 Parameter Estimation Approach

The applied forecasting model consists of four free parameters: t_a, $A\sigma_n$, r, and CV. All these parameters are assumed to be constant in space and inverted from the data (i.e.

ΔCFS values and aftershock data). Mean ΔCFS values were calculated for 15 different layers within 1 and 15 km depth and on a horizontal grid with spacing of 5km. As an example, figure 4 shows the determined stress changes at 10 km depth. We adopted the maximum likelihood method (Ogata, 1998; Daley and Vere-Jones, 2003) to fit the data. The characteristic time scale t_a for the aftershock relaxation is poorly constrained by the aftershock data, because of the ongoing aftershock decay. Our estimation of the relaxation time t_a yields a broad likelihood maximum between 40 and 70 years. To reduce the parameter space, we therefore fixed the aftershock duration time to the value of t_a = 25000 days or 65.4 years. We performed a grid search in the intervals $A\sigma_n \in [0.01, 0.2]$ MPa and CV $\in [0.5, 1.5]$ to find the best fitting values for the remaining parameters $A\sigma_n$ and CV using the maximum likelihood method. For given $A\sigma_n$ and CV, the r-value which optimizes the log-likelihood value LLmax is analytically determined by setting the derivative of the log-likelihood function with respect to r equal to zero (see Appendix of Hainzl et al., 2009).

Error bounds are defined by the minimum and maximum parameter values yielding a log-likelihood value LL=LLmax-0.5, which corresponds to plus/minus one standard deviation in the case of a normal distribution. To find these error bounds, we set the parameter to its optimal value and started to successively decrease or increase the parameter value by a small increment until the LL-value of the fit with optimized remaining parameters equaled LL=LLmax-0.5.

We evaluate the role of grid spacing in terms of model parameter estimation and found those estimated parameters are stable under sub-gridding. The results are shown in table 1. Our standard choice for the parameter estimation is the time window from 0.5 to 1000 days. However, the model parameters are also estimated for two smaller time windows: [0.5, 2.5] and [0.5, 10] days to check the consistency and robustness of the result.

Because of the loosely constrained value of t_a, we also repeat the estimations with t_a ~48 years. The results are shown in the table 2. A correlation between the background rate r and t_a is observed because for a fit on short times, r* t_a only is constrained and thus for smaller t_a, the estimate of r becomes larger (see also the figure 7; Cocco et al., 2010).

3. RESULTS FOR THE KASHMIR AFTERSHOCK SEQUENCE

The results for the parameter estimation in the case of the Kashmir's aftershock sequence are shown in table 2. All parameters were found to be already quite well constrained by the early aftershocks and remain rather stable for estimations based on much longer time intervals. Furthermore, the inverted parameter values are reasonable and very close to previous estimations. Our estimated background rate is 0.055 ± 0.002 per day for M≥3.7 which is close to the estimation of Jouanne et al. (2011) estimated for M≥3.5 (their result of 0.08 per day corresponds to 0.08 10-0.2b ≈ 0.047 M≥3.7 events per day assuming b=1.15). The estimated value of $A\sigma_n$ = 0.0185 ± 0.001 MPa is in the same order as estimations for different earthquake sequences (Toda et al., 1998; Catalli et al., 2008; Hainzl et al., 2009). Furthermore, the inverted value CV=0.94±0.01 is similar to the estimation for the Landers aftershock sequence (Hainzl et al. 2009). Note that the model accounting for stress variability significantly improves the fit which is shown by the difference between the values of the Akaike Information Criterion, ΔAIC = -2 [LL(CV=0) – LL] - 2, provided in table 2.

Using the inverted parameters, we analyze the aftershock sequence of Kashmir's mainshock in more detail. According to Parsons et al. (2012), the static stress model fails to forecast the spatial distribution of those aftershocks which occurred in the stress shadow region (i.e., in the region, where the calculated stress change induced by the major event was negative). To investigate this point, we separate the aftershock activity

in two different regions which experienced significant positive and negative stress changes due to the Kashmir event:

1. All subvolumes where the calculated stresses are positive and greater than 0.01 MPa.
2. All subvolumes where the calculated stresses are negative and less than -0.01 MPa.

The total number of aftershocks occurred in the stress shadow region are approximately two third of the aftershocks occurred in the region with increased stress. However, both volumes have different spatial size. The observed aftershock densities in these regions are plotted in figure 5 (bold lines) as a function of time. It shows that the aftershock density is significantly higher in the stressed regions than in the stress shadows. A clear Omori law decay of the aftershock activity is observed not only in the loaded regions but also in the stress shadow regions as previously observed by Mallman and Zoback (2007), indicating that activation rather than quiescence occurred. This seems to contradict the static stress-triggering hypothesis, but only if the variability of the stress calculation is ignored.

We used the inverted values $A\sigma_n$ = 0.0185 MPa, r = 0.055 (events per day), t_a = 25000 days to calculate the aftershock density with (CV = 0.94; Fig. 5a) and without stress field variability (CV = 0; Fig. 5b) in the rate-and-state model. Figure 5b shows that the estimated aftershocks decay in the regions with the highest stress increase can be well described by the model without accounting for stress field variability, but the same model completely fails for the stress shadows in agreement with the previous result based solely on static stress patterns (Parsons et al., 2012). On the other hand, after accounting for stress variability, the model fits all regions equally well. As already mentioned above, the model is also self-consistent in a way that the parameter

estimations are robust for different time intervals also suggests that secondary triggering does not effect on the estimation of CV. We have found that parameters which have been inverted for the first days of the aftershock are able to reproduce the aftershock decay also on longer time scales in stress shadows as well as in regions of stress concentration. However, as shown in figure 5, the model tends to overestimate the seismicity rate in the later stage in the region that experienced positive stress changes, while it slightly underestimates the seismicity rate in the approximately first 10 days in the region that experienced negative stress changes.

Figure 6 shows the spatial distribution of the forecasted earthquake rates calculated from the seismicity model. These maps have been calculated by integrating the forecasted earthquake rates over the first 9.5 days for the models with CV = 0.94 and CV = 0 respectively. The comparison with the epicenters of the $M \geq 3.7$ aftershocks recorded in the same time period shows that the consideration of stress variability can explain the activation of earthquake in the apparent stress shadows. We further extend our analysis to test whether the estimated model parameters, particularly CV, are biased by secondary triggering, which is supposed to play an important role as pointed out by Parsons et al. (2012). We run the simulation for the case of declustered catalogs considering the time interval [0.5 10] days. The resulting model parameters for 100 declustered aftershock catalogs are shown in the table 2. Results depict that parameter estimations are affected by secondary aftershock clustering. As examples for declustered catalogs leading to CV=0.9 and CV=1.3, we plot the stress variation versus mean stress value at the hypocenter of direct aftershocks as shown in the figure 7. The inverted values of CV from both direct aftershocks catalogs are 0.9 and 1.3 which is close to the theoretical CV as shown by the bold lines. In summary, the estimated CV-values vary from 0.8 to 1.4 meaning that removing the secondary aftershocks slightly effect the estimation of CV,

but its absolute value remains significant indicating that uncertainties related to slip model and receiver mechanisms are large. As an example, figure 8 and 9 are shown the aftershocks density in both stress increases and decreased region and spatial distribution of the forecasted earthquake rates for the case of stochastically declustered catalogs. The comparison of the model results with the observations, showing several patterns of remaining earthquakes after the declustering show that the model fit the observed data quite well.

4. DISCUSSION

Rate-and-state dependent seismicity models, which incorporate only deterministic Coulomb failure stresses computed for a particular choice of model parameters and prescribed faulting mechanisms or optimally oriented fault planes, for instance, fail to predict the increased seismicity rate often observed in stress shadows (Catalli et al., 2008; Parsons et al., 2012). However, large uncertainties are associated with those stress calculations, which have to be taken into account (Hainzl et al., 2009). These uncertainties are due to weakly constrained slip distributions, receiver fault mechanisms and crustal structures. Thus accounting only for deterministic Coulomb failure stresses is not appropriate to analyze and forecast the spatiotemporal evolution of seismicity based on rate-and-state dependent frictional earthquake nucleation. According to Hainzl et al. (2009) and also shown in this paper, the confidence intervals (standard deviation) of the calculated stress values are likely to be in the same order as of mean stress value at each location due to above mentioned uncertainties. The consideration of the broad probability distribution can explain the activation of earthquakes in the apparent stress shadow region (Helmstetter and Shaw, 2006; Marsan et al., 2006; Hainzl et al., 2009). For simplification, a Gaussian distributed probability density function defined by its

mean and standard deviation is used to account for the variability of the stress field in the model. The use of the correlated uncertainties of finite-fault source models is preferable (Woessner et al., 2012), however, these information are usually not available. Anyway, uncertainties related to the slip model can only account for a part of the involved uncertainties. Thus the applied simple approach might be reasonable in our case. By accounting for the variability of stress field (CV-value), we tested whether the aftershock occurrence triggered by the M7.6 Kashmir event can be modeled by the static stress changes and rate- and state-dependent frictional earthquake nucleation. The analysis shows consistent estimations of parameters on different time scales similar to the results of Hainzl et al. (2009) in the case of the 1992 Landers earthquake. Based on these parameters, the model is able to fit the spatiotemporal distribution of aftershocks. Furthermore, aftershocks can influence the local stress field significantly and thus lead to a non negligible number of secondary aftershocks (Ogata, 1998; Felzer et al., 2003) which might also explain apparent failures of the static stress-triggering model as pointed out by Parsons et al. (2012). To evaluate the contribution of aftershock-related stress changes in the estimation of CV-value, we have analyzed catalogs where secondary aftershocks are stochastically removed. Our analysis shows that role of secondary clustering seems to be negligible and other uncertainties e.g. related to slip model and receiver mechanisms, play a major role for this catalog. It is well known that the Asig-value together with r controls the instantaneous increase of seismicity rate: the smaller Asig and the larger r, the larger are the seismicity rate changes (Coco et al., 2010). Our results for the declustered catalogs show an increased $A\sigma_n$ value and a decreased r value consistent with the decrease of seismicity rate. However, it should be noted that ETAS-estimated value of the background rate is not well constrained because the background rate does not play a significant role in the fitting period [0.5 10] days,

where direct and secondary triggering dominates. Furthermore, also the value estimated by the CRS model is not well constrained because of the correlation between the background value and the aftershock duration time t_a (Cocco et al. 2010). It is also noted that the CRS model underestimate the seismicity rates in the stress shadow region at shorter time period [0.5 10] days as sown in the figures 5 and 8. This might be the result of not having deterministic knowledge and ignoring dynamic stress triggering. However, the model explains the seismicity rate at longer time period [10 1000] days well. This is also indicated by Segou et al. (2013). It is important to note that a number of simplifications were made in this study, in particular, the background rate was assumed to be constant in space, because its estimation from limited catalog data can introduce large uncertainties which can lead to a worsening of the fit. This has been demonstrated for the Coulomb-Rate-State model by Cocco et al. (2010), but holds similarly for the ETAS model. However, in reality, the background rate is most likely variable in space as preexisting fault structures are associated with higher background rate than those regions without these features (Toda and Stein, 2003; Zhuang et al., 2002; Toda et al., 2005). The estimated CV-value might thus also compensate some of the unresolvable spatial variability of background rates as well as $A\sigma_n$ and t_a parameters occurring in reality. Finally, it is important to note that the spatiotemporal distribution of aftershocks can be influenced by time dependent post-seismic processes such as induced fluid flow and afterslip (Cattania et al., 2015), which has been ignored in our study.

5. CONCLUSION

Seismicity models built on static Coulomb stress changes often fail to explain a large part of the aftershock activity. This might be explained by the large uncertainties associated with stress calculations and the nonlinear response of earthquake nucleation

to stress changes. To explore this possibility for the specific aftershock sequence following the 2005 M7.6 Kashmir event, we applied the physics-based statistical model introduced by Dieterich (1994) which is built on the basis of static Coulomb stress changes and rate-and-state dependent friction laws to forecast the spatiotemporal distribution of the aftershock activity. We approximated stress uncertainties by Gaussian-distributed stress values, where the standard deviation is assumed to be equal to be CV times the mean value. The values of the different model parameters (i.e. $A\sigma_n$, r and CV) used in this model approach were estimated by maximum likelihood fitting to the data. The resulting values are found to be reasonable. The estimated value $A\sigma_n$ =0.0185±0.001 MPa is in the range of previously observed values between 0.01 and 0.2 MPa for other aftershock sequences and the estimated value of the background seismicity rate is similar to the estimation of Jouanne et al. (2011). Furthermore, the coefficient of stress variation (CV) is estimated as 0.94±0.01, which is close to previously estimated values by Hainzl et al. (2009) and Marsan et al. (2006). For the case of declustered catalogs, we found that estimated value of CV increases to 1.1±0.3 indicating that stress-changes induced by aftershocks contribute only a minor part to the overall uncertainties of the stress calculations which have to be considered in stress-based seismicity models. The consistency of the model is not only demonstrated by the reasonable parameter estimations, but also by the observation that the estimations are robust for different time intervals. Based on the inverted parameters, the model is found to explain most of the spatiotemporal seismicity patterns well, even the activation in apparent stress shadows. Thus our result indicates that stress heterogeneity plays an important role in the activation of aftershocks in the stress shadow region.

ACKNOWLEDGMENTS:

This work is partly funded by the Generali Group. Comments by Tom Parsons and one

anonymous reviewer improved the manuscript.

REFERENCES:

1. Avouac, J. P., Ayoub, F., Leprince, S., Konca, O. and Helmberger, D. V. (2006), The 2005, Mw 7.6 Kashmir earthquake: Sub-pixel correlation of ASTER images and seismic waveforms analysis, Earth Planet. Sci. Lett., 249, 514–528, doi:10.1016/j.epsl.2006.06.025.

2. Catalli, F., Cocco, M., Console, R. and Chiaraluce, L. (2008), Modeling seismicity rate changes during the 1997 Umbria-Marche sequence (central Italy) through rate and state dependent model, J. Geophys. Res., 113, B11301, doi:10.1029/2007JB005356.

3. Cattania, C., S. Hainzl, L. Wang, F. Roth, and B. Enescu (2014), Propagation of Coulomb stress uncertainties in physics-based aftershock models, J. Geophys. Res. Solid Earth, 119, 7846–7864, doi:10.1002/2014JB011183.

4. Cattania, C., S. Hainzl, L. Wang, B. Enescu, and F. Roth (2015), Aftershock triggering by postseismic stresses: A study based on Coulomb rate-and-state models, J. Geophys. Res. Solid Earth, 120, 2388–2407, doi:10.1002/2014JB011500.

5. Cocco, M., Hainzl, S., Catalli, F., Enescu, B., Lombardi, A. M. and Woessner, J. (2010), Sensitivity study of forecasted aftershock seismicity based on Coulomb stress calculation and rate- and state-dependent frictional response, J. Geophys. Res., 115, B05307, doi:10.1029/2009JB006838.

6. Daley, D. J. and Vere-Jones, D. (2003), An Introduction to the Theory of Point Processes, Vol. I: Elementary Theory and Methods, 2nd ed., Springer, New York.

7. Dieterich, J. H. (1992), Earthquake nucleation on faults with rate-and State-dependent friction, Tectonophysics, 211, 115–134

8. Dieterich, J. H. (1994), A constitutive law for rate of earthquake production and its application to earthquake clustering, J. Geophys. Res., 99 (B2), 2601–2618.

9. Dieterich, J. H., Cayol, V. and Okubo, P. (2000), The use of earthquake rate changes as a stress meter at Kilauea volcano, Nature, 408, 457–460.

10. Felzer, K. R., Abercrombie, R. E. and Ekstrom, G. (2003), Secondary aftershocks and their importance for aftershock forecasting, Bull. Seismol. Soc. Am., 93(4), 1433– 1448.

11. Gardner, J. K., and Knopoff, L. (1974), Is the sequence of earthquakes in Southern California, with aftershocks removed, Poissonian?, Bull. Seismol. Soc. Am., 64(5), 1363-1367.

12. Hainzl, S., Enescu, B., Cocco, M., Woessner, J., Catalli, F., Wang, R. and Roth, F. (2009), Aftershock modeling based on uncertain stress calculations, J. Geophys. Res., 114, B05309, doi: 10.1029/2008JB006011, 2009.

13. Hainzl, S., Steacy, S. and Marsan, D. (2010a), Seismicity models based on Coulomb stress calculations, Community Online Resource for Statistical Seismicity Analysis, doi:10.5078/corssa-32035809.

14. Hainzl, S., Zöller, G. and Wang, R. (2010b), Impact of the receiver fault distribution on aftershock activity, J. Geophys. Res., 115, B05315, doi:10.1029/2008JB006224.

15. Hardebeck, J. L. and Hauksson, E. (2001), Crustal stress field in southern California and its implications for fault mechanisms, J. Geophys. Res., 106 (B10), 21, 859– 21, 882.

16. Harris, R. A. (1998), Introduction to special section: stress triggers, stress shadows, and implication for seismic hazard. J. Geophys. Res., 103, 24 347-24, 358.

17. Harris, R. A. and Simpson, R. W. (1992), Changes in static stress on southern California faults after the 1992 landers earthquake. Nature, 360, 251-254.

18. Helmstetter, A. and Shaw, B. E. (2006), Relation between stress heterogeneity and aftershock rate in the rate-and-state model, J. Geophys. Res., 111, B07304, doi:10.1029/2005JB004077.

19. Jouanne, F., Awan, A., Madji, A., Pêcher, A., Latif, M., Kausar, A., Mugnier, J. L., Khan, I. and Khan, N. A. (2011), Postseismic deformation in Pakistan after the 8th October 2005 earthquake: Evidence of afterslip along a flat north of the Balakot-Bagh thrust, J. Geophys. Res., 116, B07401, 22 PP.,doi:10.1029/2010JB007903.

20. Kagan, Y. Y. (2004), Short-term properties of earthquake catalogs and models of earthquake source, Bull. Seismol. Soc. Am., 94 (4), 1207–1228.

21. King, G. C. P., Stein, R. S. and Lin, J. (1992), Change in failure stress on the southern San Andreas fault system caused by the 1992 magnitude = 7.4 Landers earthquake. Science, 258, 1328-1332.

22. Mallman, E. P. and Zoback, M. D. (2007), Assessing elastic Coulomb stress transfer models using seismicity rates in southern California and

southwestern Japan, J. Geophys. Res., 112, B03304, doi:10.1029/2005JB004076.

23. Marsan, D. (2006), Can coseismic stress variability suppress seismicity shadows? Insights from a rate-and-state friction model, J. Geophys. Res., 111, B06305, doi:10.1029/2005JB004060.

24. Ogata, Y. (1988), Statistical models for earthquake occurrences and residual analysis for point processes, J. Am. Stat. Assoc., 83, 9–27.

25. Ogata, Y. (1992), Detection of precursory relative quiescence before great earthquakes through a statistical model, J. Geophys. Res., 97, 19845–19871.

26. Ogata, Y. (1998), Space-time point-process models for earthquake occurrences, Ann. Inst. Stat. Math., 50, 379–402.

27. Okada, Y. (1992), Internal deformation due to shear and tensile faults in a half space, Bull. seism. Soc. Am., 82, 1018–1040.

28. Parsons, T., Ogata, Y., Zhuang, J. and Geist, E. L. (2012), Evaluation of static stress change forecasting with prospective and blind tests, Geophys. J. Int., 188, 1425–1440, doi: 10.1111/j.1365-246X.2011.05343.x

29. Parsons, T., Yeats, R. S., Yagi, Y. and Hussain, A. (2006), Static stress change from the 8 October, 2005 M = 7.6 Kashmir earthquake, Geophys. Res. Lett., 33, L06304, doi:10.1029/2005GL025429.

30. Pathier, E., Fielding, E. J., Wright, T. J., Walker, R., Parsons, B. E. and Hensley, S. (2006), Displacement field and slip distribution of the 2005 Kashmir earthquake from SAR imagery, Geophys. Res. Lett., 33, L20310, doi:10.1029/2006GL027193.

31. Reasenberg, P. A. and Simpson, R. W. (1992), Response of regional seismicity to the static stress change produced by the Loma Prieta earthquake, Science, 255:1687-1690.

32. Rice, J. R. and Cleary, M. P. (1976), Some basic stress diffusion solutions for fluid-saturated elastic porous media with compressible constituents, Reviews of Geophysics and Space Physics, 14:227-241.

33. Segou, M., T. Parsons and W. Ellsworth (2013), Comparative evaluation of combined physics based and statistical forecast models, Journal of Geophysical Research, v. 118, p. 6219-6240, doi:10.1002/2013JB010313.

34. Stein, R. S. (1999), The role of stress transfer in earthquake occurrence, Nature, 402(6762), 605–609.

35. Stein R. S., Lin, J. and King, G. C. P. (1981), Static stress changes and the triggering of earthquakes. Bull. Seismol. Soc. Am., 84:935-953.

36. Stein, R. S. and Lisowski, M. (1983), The 1979 Homestead valley earthquake sequence California: Control of aftershocks and postseismic deformation. J. Geophys. Res., 88:6477-6490.

37. Stiphout, T., Zhuang, T. and Marsan, J. D. (2010), Seismicity Declustering, Community Online Resource for Statistical Seismicity Analysis, doi:10.3929/ethz-a-xxxxxxxxx.

38. Toda, S., Stein, R. S., Reasenberg, P. A., Dieterich, J. H. and Yoshida, A. (1998), Stress transferred by the 1995,Mw = 6.9 Kobe, Japan, shock: Effect on aftershocks and future earthquake probabilities, J. Geophys. Res., 103 (B10), 24,543–24,565.

39. Toda, S., and Stein, R. S. (2003), Toggling of seismicity by the 1997 Kagoshima earthquake couplet: A demonstration of time dependent stress transfers J. Geophys. Res., 108(B12), 2567, doi:10.1029/2003JB002527.

40. Toda, S., Stein, R. S., Richards-Dinger, K. and Bozkurt, S. B. (2005), Forecasting the evolution of seismicity in southern California: Animations built on earthquake stress transfer, J. Geophys. Res., 110(B5),

B05S16, doi:10.1029/2004JB003415.

41. Utsu, T. (1961), A statistical study on the occurrence of aftershocks, Geophys. Mag., 30, 521605.

42. Woessner, J., S. Hainzl, W. Marzocchi, M. J. Werner, A. M. Lombardi, F. Catalli, B. Enescu, M. Cocco, M. C. Gerstenberger, and S. Wiemer (2011), A retrospective comparative forecast test on the 1992 Landers sequence, J. Geophys. Res., 116, B05305, doi:10.1029/2010JB007846.

43. Woessner, J., Jonsson, S., Sudhaus, H. and Bachmann, C. (2012), Reliability of Coulomb stress changes inferred from correlated uncertainties of finite-fault source models, J. Geophys. Res., 117, B07303, doi:10.1029/2011JB009121.

44. Zhuang, J., Ogata, Y. and Vere- Jones, D. (2002), Stochastic declustering of time earthquake occurrences, J. Am. Stat. Assoc., 97, 369–380.

45. Zhuang, J., Ogata, Y. and Vere- Jones, D. (2004), Analyzing earthquake clustering features by using stochastic reconstruction, J. Geophys. Res., 109, B05301, doi:10.1029/2003JB002879.

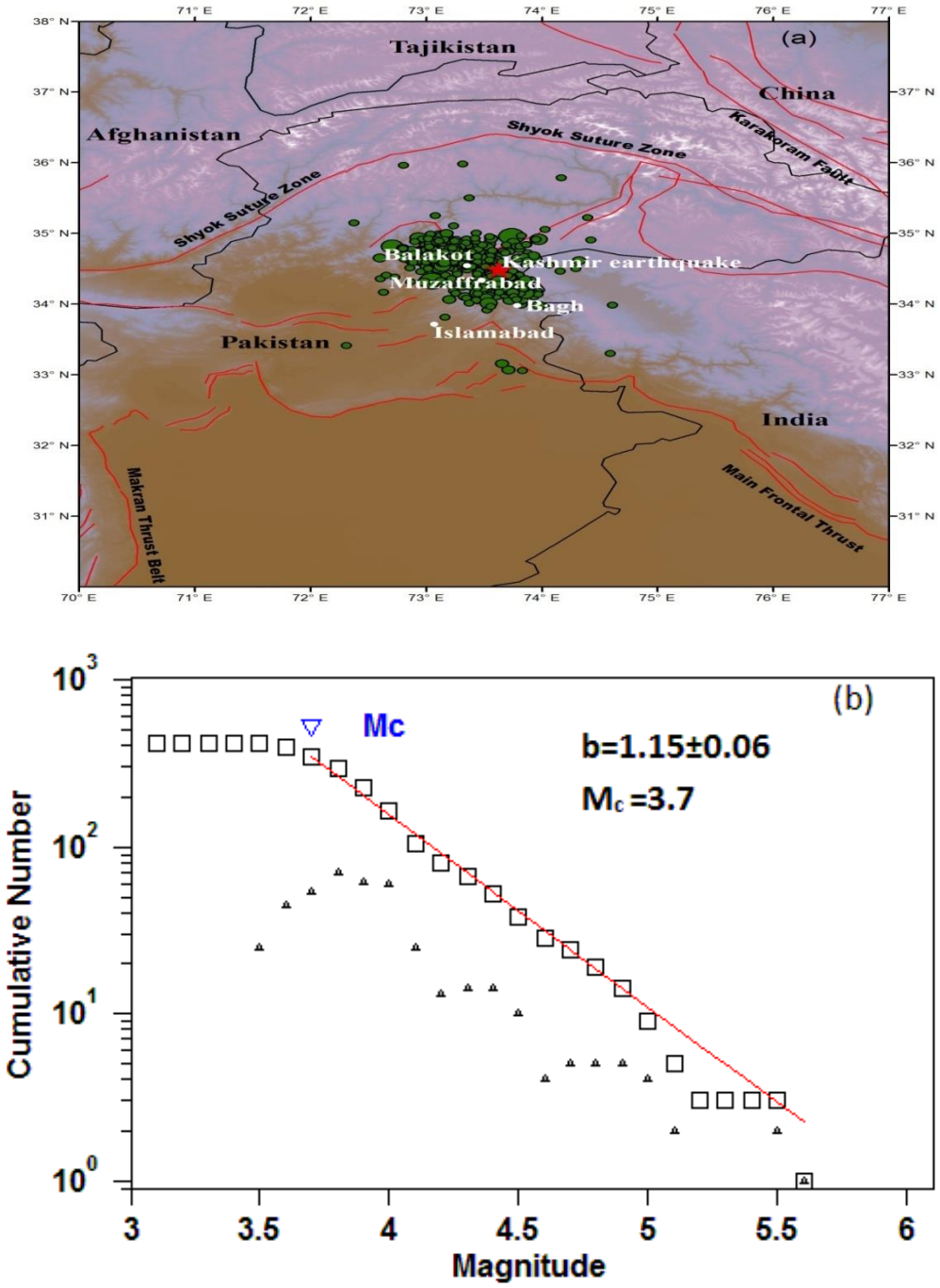

Figure1: (a) Map shows the aftershocks of Oct 8, 2005 earthquake where the red star indicates the epicenter of the mainshock, (b) frequency-magnitudedistribution(FMD) of aftershocks for t>0.5 days with b=1.15±0.06 and magnitude of completeness Mc=3.7. Triangles and squares represent the number and cumulative number of each individual magnitude level of earthquake, respectively. The line represents the FMD linear regression fitted with the observed data.

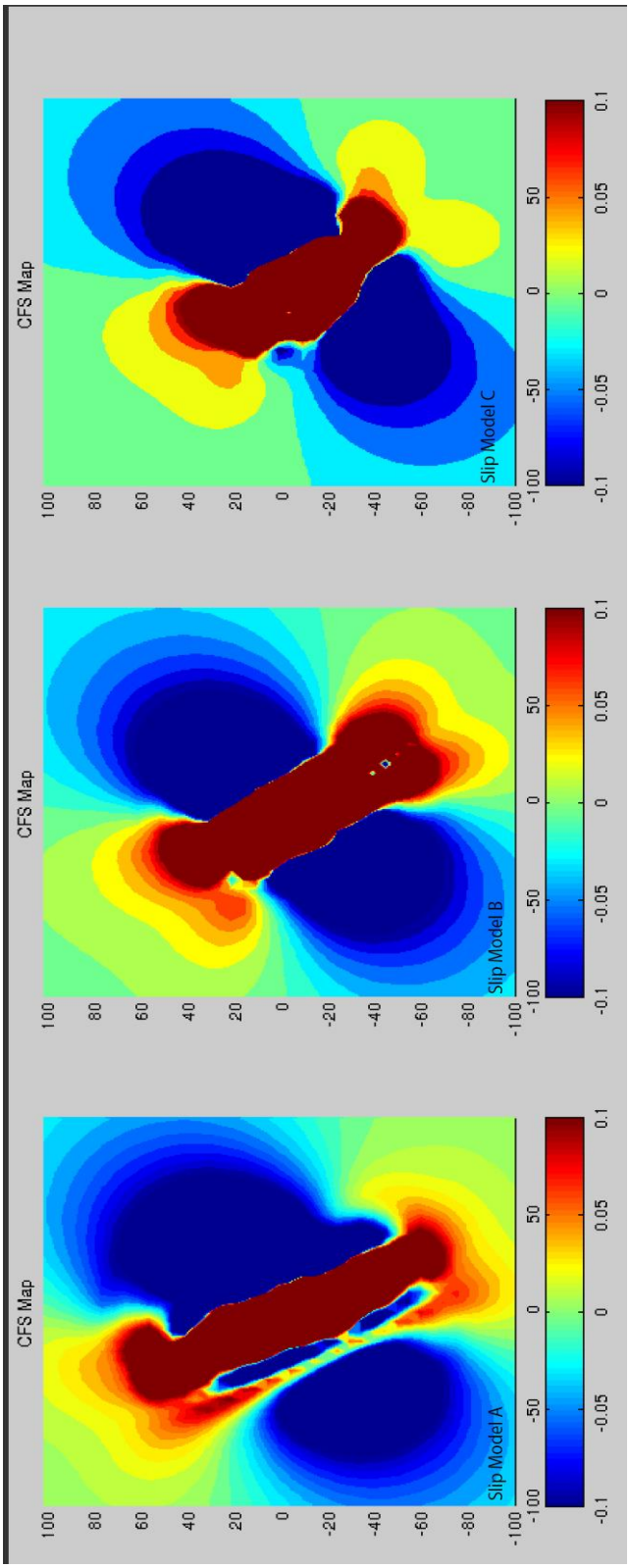

Figure 2: Coulomb failure stresses computed at 10km depth using three used slip models with coefficient of friction μ=0.4

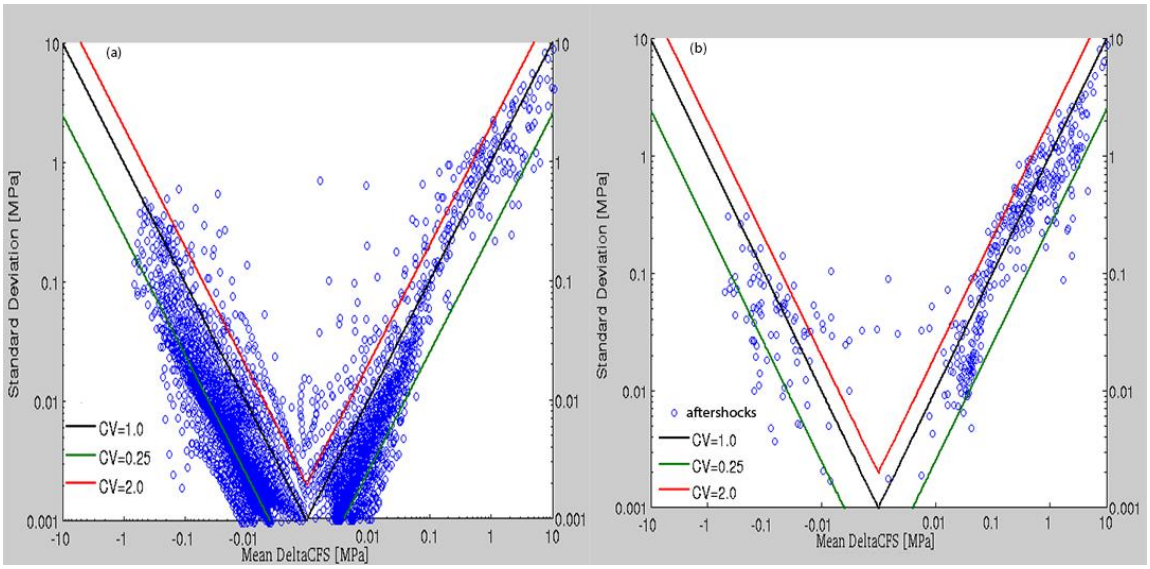

Figure 3: Standard variation of calculated stress changes as a function of the mean stress change computed from three slip models. The result is plotted for the locations: a) where we have computed the stress changes at 10km depth and b) at the hypocenter of the aftershocks. The lines correspond to different values of the coefficient of variation CV.

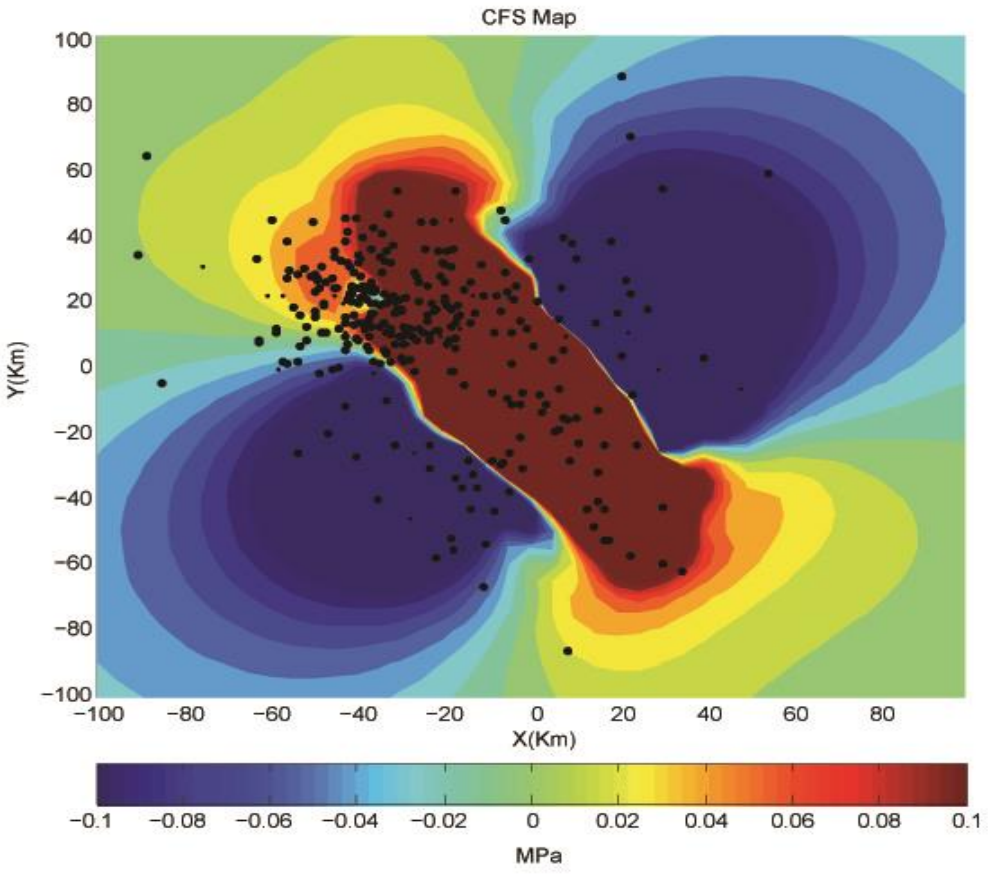

Figure 4: The Coulomb Failure Stress (ΔCFS) calculated at 10km depth with μ'=0.4 assuming optimally oriented fault planes. Black dots refer to M≥3.7 aftershocks in the time period 0.5-10 days.

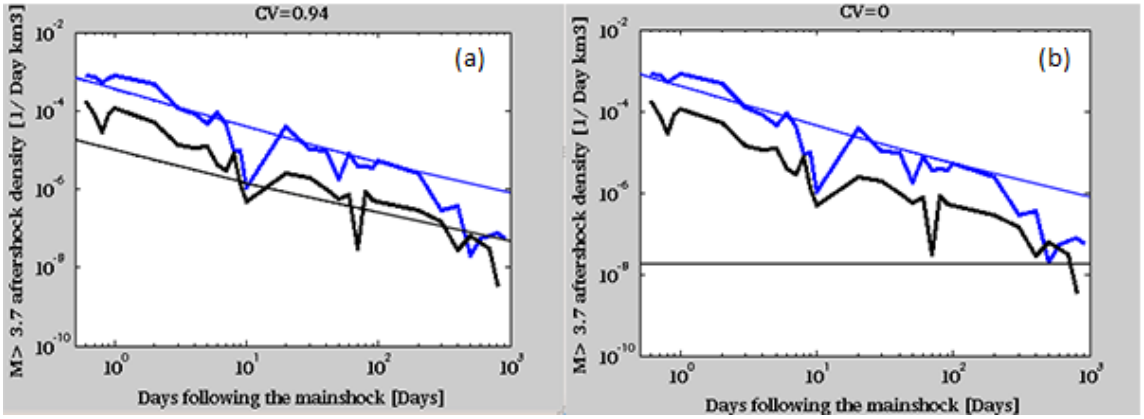

Figure 5. Comparison of the observed Kashmir's aftershock activity (bold lines) with that of the Coulomb rate-and-state model (thin lines): (a) with (CV=0.94) and (b) without (CV=0) consideration of stress heterogeneities. Blue and black curves are related to the earthquake density in regions with significant positive (ΔCFS>0.01 MPa) and negative (ΔCFS<-0.01MPa) stress changes, respectively. Model results were calculated with t_a =25,000 days, $A\sigma_n$ =0.0185 MPa and r=0.055 events/day

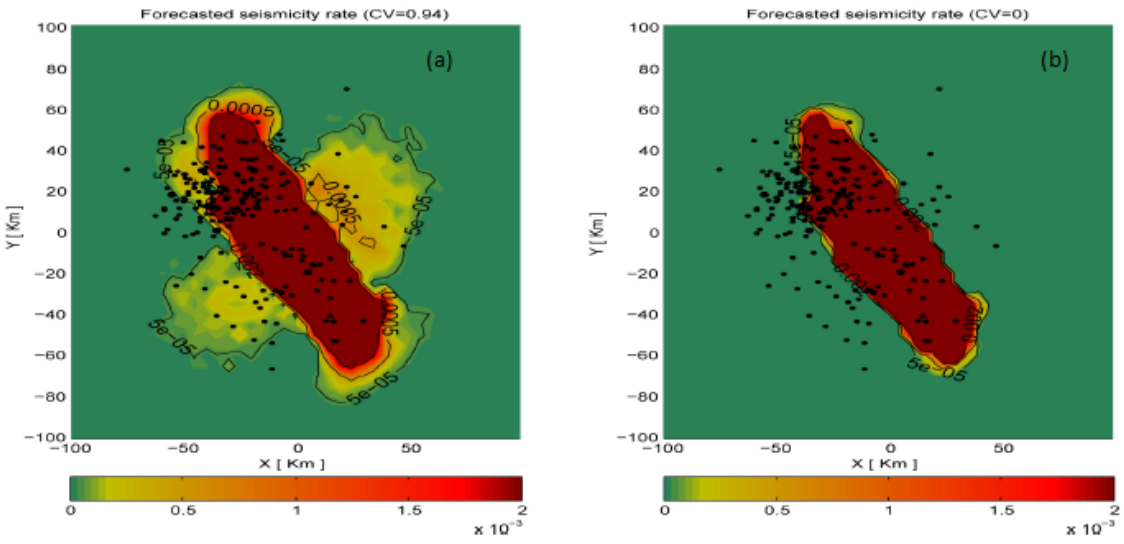

Figure 6: Spatial distribution of the aftershock rates (per 5km times 5km cell) forecasted by the model in comparison with the observed M≥3.7 aftershocks (dots) for the time interval [0.5, 10] days: (a) CV=0.94 and (b) CV=0. The other parameters are t_a =25,000 days, $A\sigma_n$ =0.0185 MPa and r=0.055 events/day.

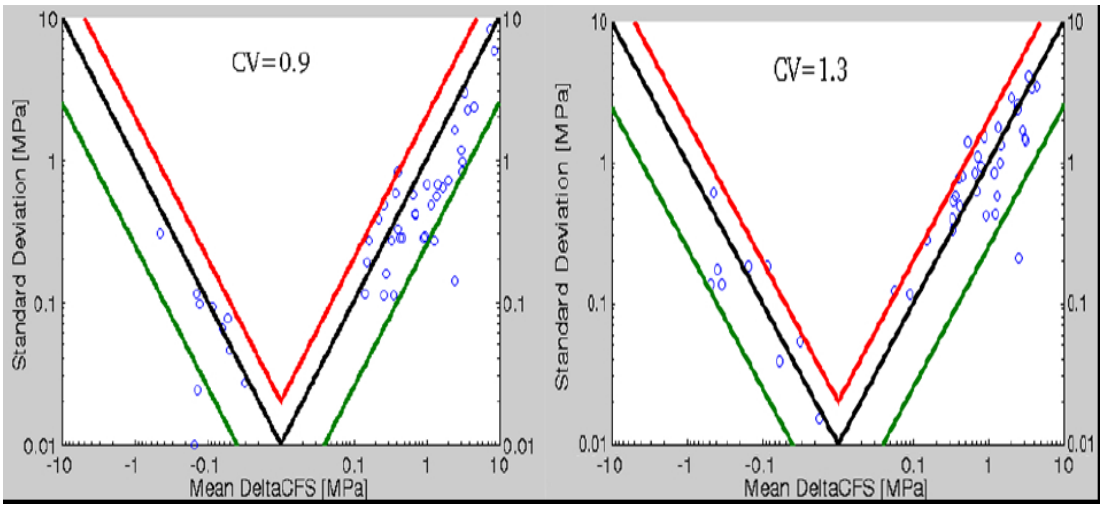

Figure 7: Standard variation of calculated stress changes as a function of the mean stress change at the hypocenter of the aftershocks for the cases of direct aftershocks with estimated CV=0.9 and CV=1.3. The lines correspond to different values of the coefficient of variation CV (the values are same as that of figure 3).

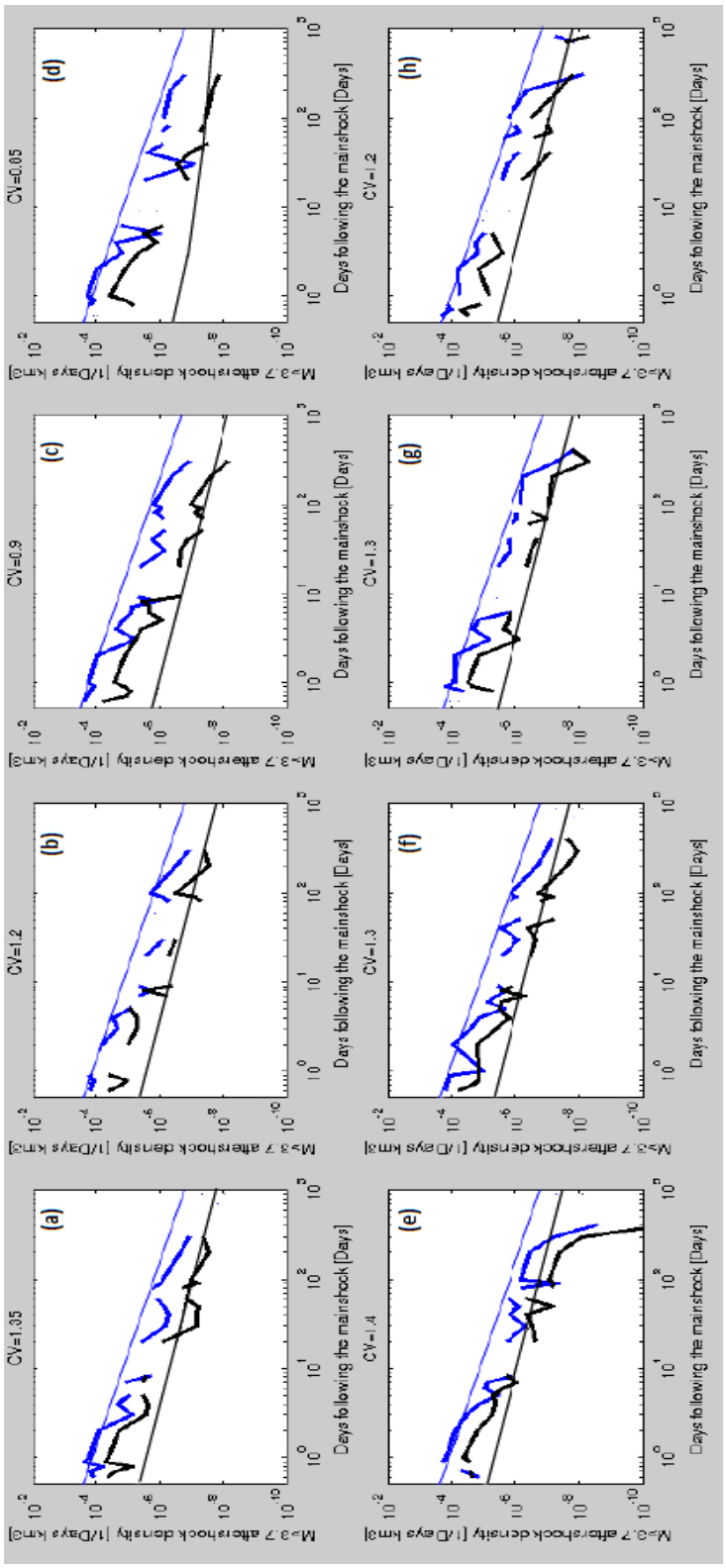

Figure 8. Comparison of the some stochastically declustered Kashmir aftershock activity (bold lines) with that of the Coulomb rate-and-state model (thin lines). Blue and black curves are related to the earthquake density in regions with significant positive (ΔCFS>0.01 MPa) and negative (ΔCFS<-0.01MPa) stress changes, respectively. Model results were calculated with t_a =25,000 and optimal values of Asig and r for each declustered catalog.

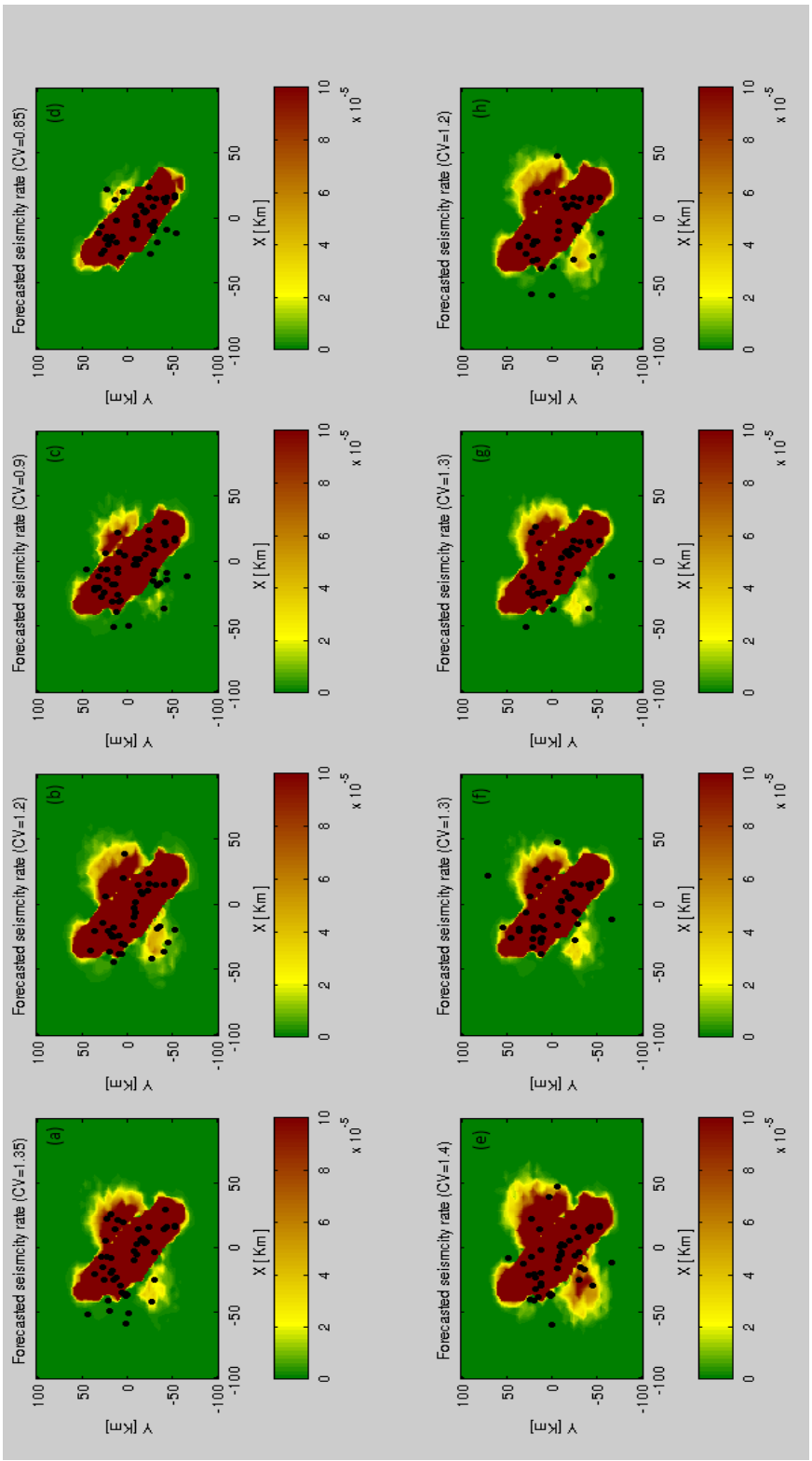

Figure 9: Spatial distribution of the aftershock rates (per 5km times 5km cell) forecasted by the model in comparison with the observed M≥3.7 aftershocks (dots) for the time interval [0.5, 10] days for the same stochastically declustered catalogs

Table 1: Estimated model parameters using 5km and 2.5km grid spacing for Coulomb stress calculation without considering uncertainties.

Aftershock time period (days) [0.5 1000]	$A\sigma_n$ (MPa)	r (events/day)	Log likelihood value
Grid-spacing: 2.5 km	0.028	0.072	-5141
Grid-spacing: 5km	0.031	0.0644	-4739

Table 2: Estimated model parameters using the original catalog and 100 stochastically declustered catalogs. ΔAIC refers to the difference between the value of the Akaike Information Criterion for the model without and with consideration of stress uncertainties. D refers to 100 stochastically deculstered catalogs.

t_a (Days)	Aftershock time period (days)	$A\sigma_n$ (MPa)	r (events/day)	CV	ΔAIC	Remarks
25000	[0.5 2.5]	0.012±0.001	0.1±0.002	0.95±0.02	287	Original Catalog
	[0.5 10]	0.017±0.001	0.095±0.003	0.96 ±0.03	324	
	[0.5 1000]	0.0185±0.001	0.055±0.002	0.94±0.01	360	
17500	[0.5 1000]	0.019±0.0015	0.103±0.004	0.92±0.02	349	
25000	[0.5 10]	0.0525 ±0.02	0.026±0.006	1.1±0.3	26	D